Biophysical Journal, Volume *110*

Supplemental Information

Relative Orientation of POTRA Domains from Cyanobacterial Omp85 Studied by Pulsed EPR Spectroscopy

Reza Dastvan, Eva-Maria Brouwer, Denise Schuetz, Oliver Mirus, Enrico Schleiff, and Thomas F. Prisner

Relative orientation of POTRA domains from cyanobacterial Omp85 studied by pulsed EPR spectroscopy

Reza Dastvan[1,2,‡,#], Eva-Maria Brouwer[3,‡], Denise Schuetz[1,2], Oliver Mirus[3], Enrico Schleiff[2-4,*] and Thomas F. Prisner, [1,2,*]

1 Institute of Physical and Theoretical Chemistry and Center for Biomolecular Magnetic Resonance, 2 Cluster of Excellence Macromolecular Complexes, 3 Molecular Cell Biology of Plants, 4 Buchmann Institute for Molecular Life Sciences, Goethe University Frankfurt, Frankfurt am Main, Germany

Supporting Figures

Supporting Figure 1. EPR on singly-labeled POTRA domains.

Supporting Figure 2. Impact of cryoprotectants and freezing conditions on PELDOR results.

Supporting Figure 3. Intra-POTRA domain distance constraints of individual POTRA domains.

Supporting Figure 4. Comparison of background-corrected PELDOR time traces of intra-POTRA domain distances of individual POTRA domains with simulated intramolecular dipolar evolution functions.

Supporting Figure 5. Comparison of intra-POTRA domain distance distributions generated by various methods.

Supporting Figure 6. Root Mean Square Fluctuations (RMSFs) for individual POTRA domains.

Supporting Figure 7 Multiple sequence alignment of POTRA domains of *ana*Omp85 and *ec*BamA.

Supporting Figure 8. PELDOR data analysis of inter-POTRA domain distances.

Supporting Figure 9. Comparison of experimentally obtained inter-domain distance distributions with distributions generated by MMM and MtsslWizard.

Supporting Figure 10. Comparison of inter-POTRA domain PELDOR time traces generated by MMM and MtsslWizard with experimental traces.

Supporting Figure 11. Comparison of experimentally obtained inter-POTRA domain distance distributions with distance distributions generated by rotamer libraries from Sezer and Hubbell.

Supporting Figure 12. Comparison of inter-POTRA domain PELDOR time traces generated by rotamer libraries from Sezer and Hubbell.

Supporting Figure 13. Comparison of experimentally obtained inter-POTRA domain distance distributions with those generated by rotamer libraries optimized for chi1 and chi3 angles from Sezer.

Supporting Figure 14. Comparison of inter-POTRA domain PELDOR time traces generated by rotamer libraries optimized for chi1 and chi3 angles from Sezer.

Supporting Figure 15. Comparison of simulated PELDOR time traces from rigid body refinement with experimental traces.

Supporting Figure 16. Comparison of simulated distance distributions from MD simulations and rigid body refinement.

Supporting Figure 17. Orientational space of POTRA domains of *in silico* spin-labeled Alr2269 sampled by MD simulations and Rosetta.

Supporting Figure 18. Predicted flexibility in POTRA domain pair *ana*P1-*ana*P2.

Supporting Tables

Supporting Table S1. Oligonucleotides used for QuickChange PCR

Supporting Table S2. Comparison of PELDOR distance constraints with X-ray structure, MD and the best refined model of either rigid body or Rosetta refinement.

Supporting Table S3. Comparison of simulated distance constraints obtained for different rotamer libraries.

Supporting Table S4. Structural similarities of POTRA domains of anaOmp85 and BamA.

Supporting Table S5. Angles and scores of top 100 Rosetta models.

Supporting References

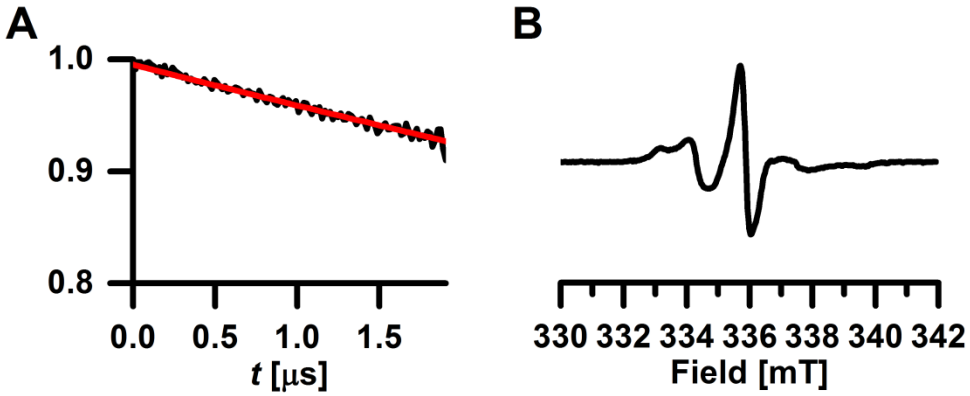

Supporting Figure 1. EPR on singly-labeled POTRA domains. POTRA domain P2 was labeled at position V370. (A) A monotonously decaying signal was observed, indicating the absence of specific inter-molecular interactions. (B) The cw-spectrum is indicative of a slow motion regime, and thus a hindered flexibility of the SL at this position.

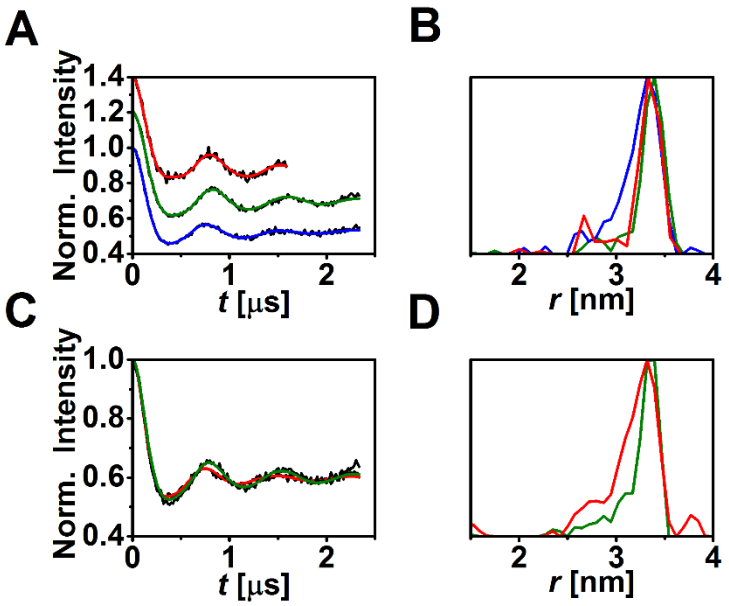

Supporting Figure 2. Impact of cryoprotectants and freezing conditions on PELDOR results. (A, B) Effect of different cryoprotectants on PELDOR measurements of the labeled mutant I292C/V370C. The background-corrected PELDOR time traces (A) and obtained distance distributions for different hydrophobic or hydrophilic cryoprotectants (B) is shown for 30% DMSO (red, 3.3±0.2 nm), 30% ethylene glycol (green, 3.4±0.2 nm), and 25% Ficoll 70 (blue, 3.3±0.3 nm). (C, D) Effect of different freezing procedures on PELDOR measurements of the I292C/V370C mutant. The background-corrected PELDOR time traces (C) and obtained distance distributions (D) for fast freezing of the samples by freeze-quench technique: with 30% glycerol (green, 3.2±0.2 nm), without glycerol (red, 3.2±0.4 nm). Likewise, no change was observed for different pH values (6–8, 3.3±0.2 nm; data not shown), and ionic strength (125–500mM NaCl, 3.3±0.2 nm; data not shown).

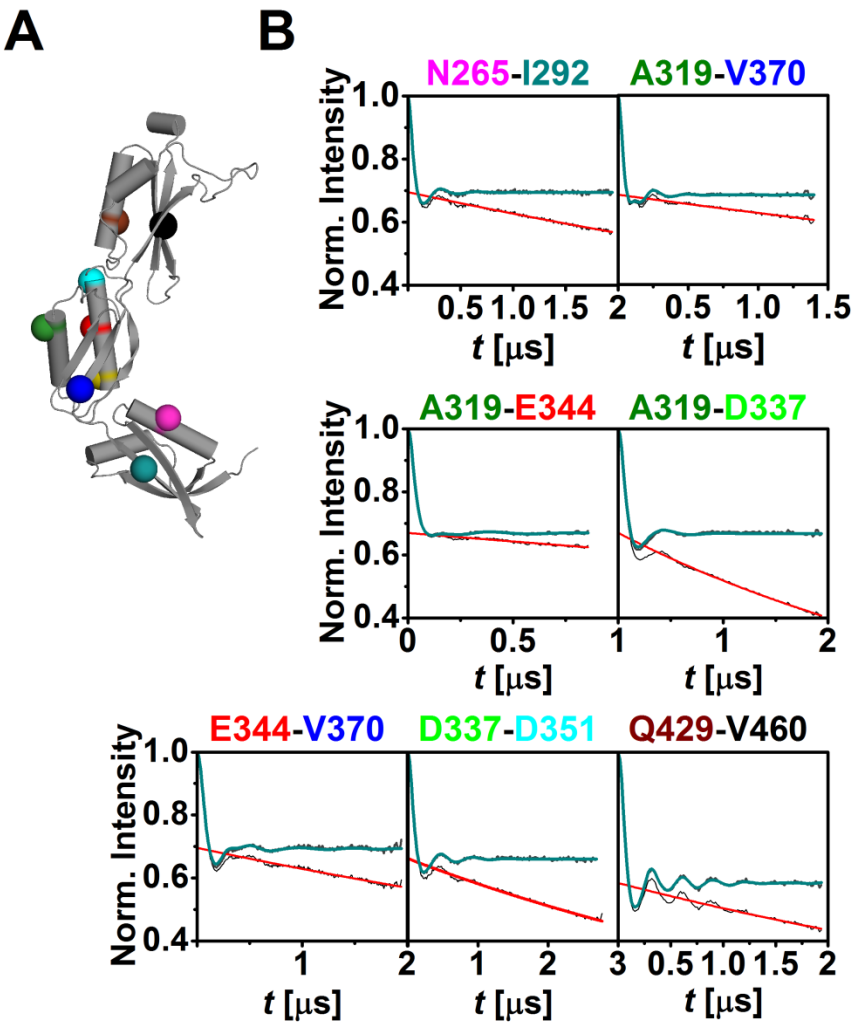

Supporting Figure 3. Intra-POTRA domain distance constraints of individual POTRA domains. (A) The crystal structure of the anaOmp85 POTRA domains indicating the spin-labeled residues. (B) The primary and background-corrected PELDOR time traces for measurements on the intra-domain double mutants with fits from Tikhonov regularization (cyan). The 3D backgrounds are shown in red.

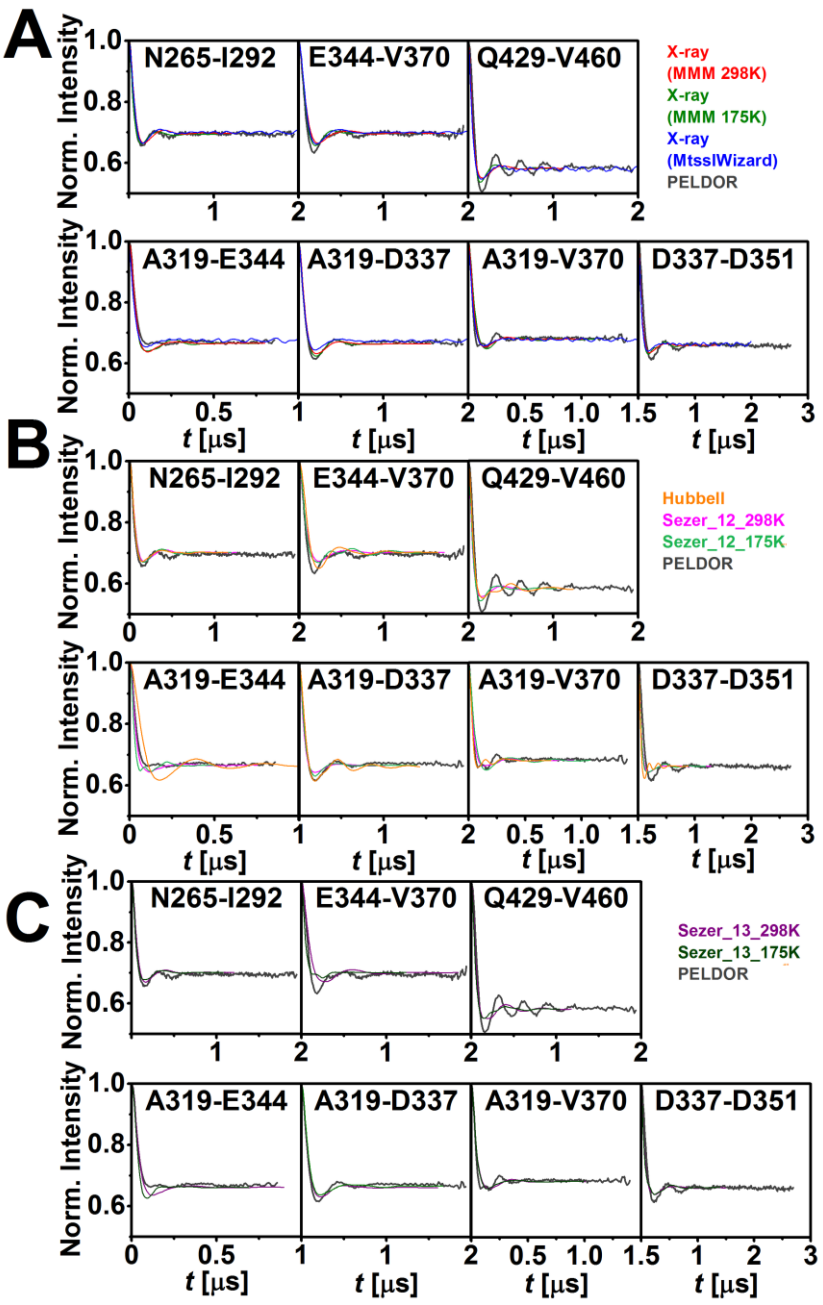

Supporting Figure 4. Comparison of background-corrected PELDOR time traces of intra-POTRA domain distances of individual POTRA domains with simulated intramolecular dipolar evolution functions. (A) Background-corrected PELDOR time traces generated on X-ray structure by MMM in 298 K mode (red), 175 K mode (green) and mtsslWizard using thorough search and loose vdW restraints (blue). (B) Background-corrected PELDOR time traces generated on X-ray structure by MMM using rotamer libraries optimized for chi1 and chi2 angles from Sezer et al. (41) at 298 K (magenta) and 175 K (light green), as well as rotamer libraries from Hubbell et al. (58) (orange). (C) Background-corrected PELDOR time traces generated on X-ray structure by MMM in using rotamer libraries optimized for chi1 and chi3 angles from Sezer et al. (41) at 298K (violet) and 175K (dark green).

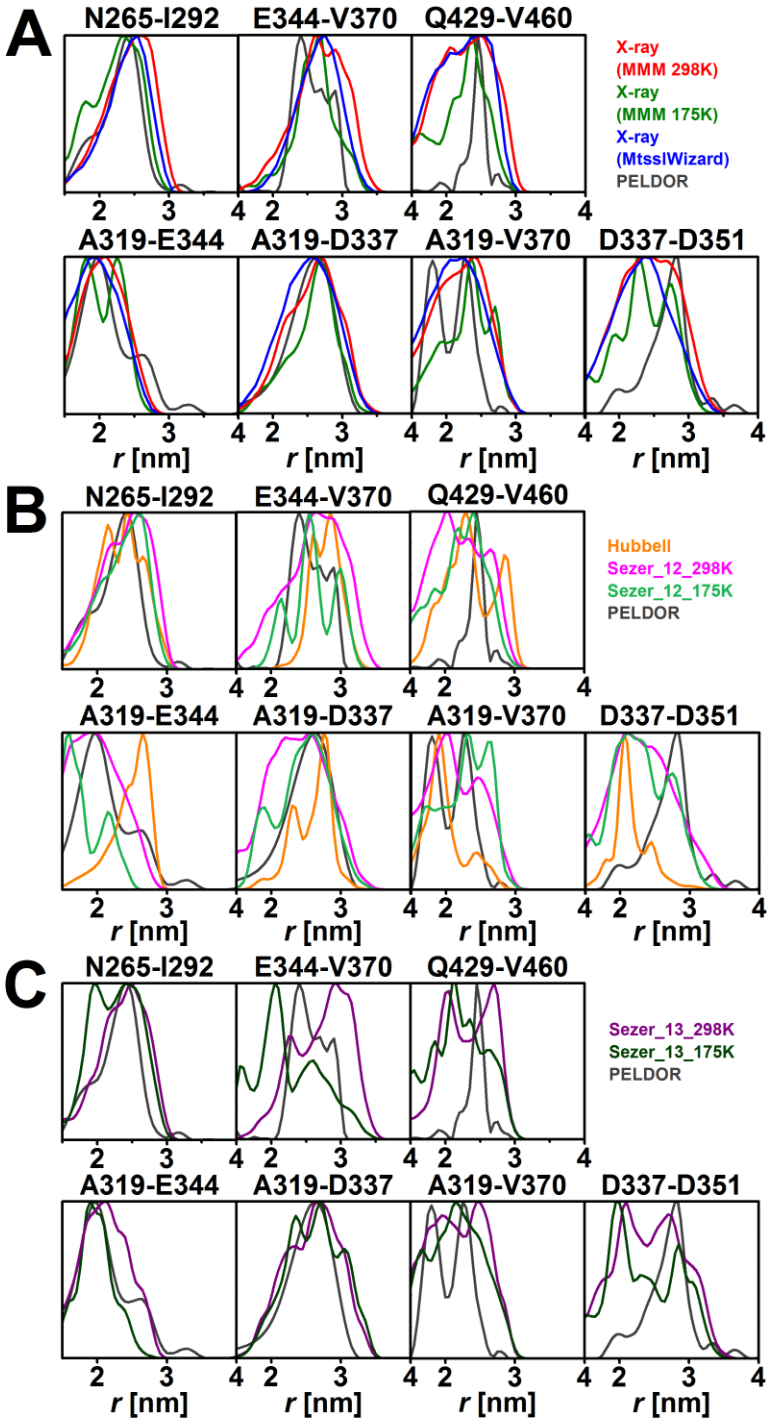

Supporting Figure 5. Comparison of intra-POTRA domain distance distributions generated by various methods. (A) Comparison of distance distributions generated on X-ray structure by MMM in 298 K mode (red), MMM in 175 K mode (green) and mtsslWizard using thorough search and loose vdW restraints (blue). (B) Comparison of distance distributions generated on X-ray structure by MMM using rotamer libraries optimized for chi1 and chi2 angles from Sezer et al. (41) at 298K (magenta) and 175K (light green) as well as rotamer library from Hubbell et al. (58) (orange). (C) Comparison of distance distributions generated on X-ray structure by MMM in using rotamer libraries optimized for chi1 and chi3 angles from Sezer et al. (41) at 298K (violet) and 175K (dark green).

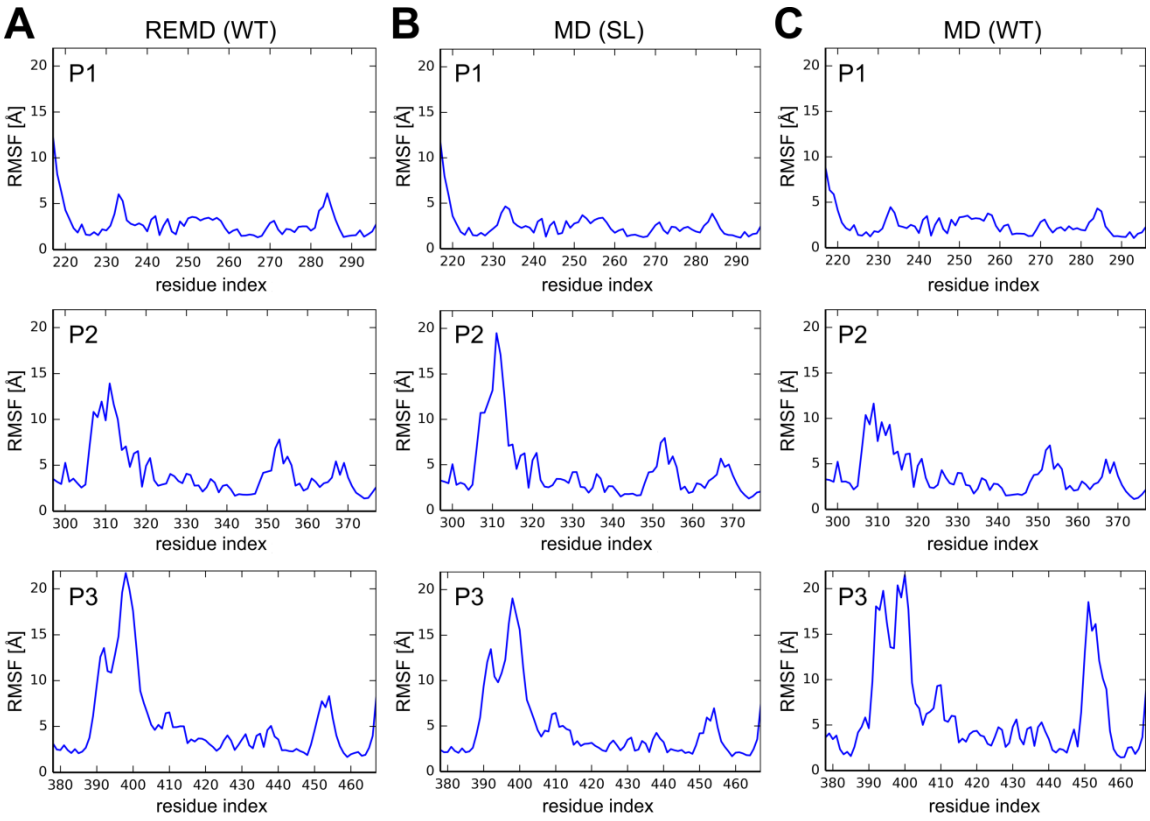

Supporting Figure 6. Root Mean Square Fluctuations (RMSFs) for individual POTRA domains.

The RMSF was calculated for all Cα atoms of each POTRA domain of *ana*Omp85 for the (A) wild-type REMD, (B) spin-labeled as well as (C) wild-type MD simulations. The residue indices correspond to the full-length protein.

```
Ana1_P1  221 VLVSEV--LVR---PQSGQ---------LTPELETQVYNVI---RTQPG---------RTTTRSQL 260
Ana1_P2  297 PVLSKV--EIQANP---GTNV-----P--SVLPQATADEIF---RAQYG---------KILNLRDL 338
Ana1_P3  379 -VVENISVRFRNE----GQDVNEQGQPIRGRTQDYIITREV---ELKPG---------QVFNRNTV 428
Ecol_P1   24 FVVKDI--HFE------GL----------QRVAVGAALLSM---PVRTG---------DTVNDEDI  59
Ecol_P2   92 PTIASI--TFS------GN----------KSVKDDMLKQNLEASGVRVG---------ESLDRTTI 130
Ecol_P3  175 AEIQQI--NIV------GN----------HAFTTDELISHF---QLRDEVPWWNVVGDRKYQKQKL 219
Ecol_P4  266 YKLSGV--EVS------GN----------LAGHSAEIEQLT---KIEPG---------ELYNGTKV 301
Ecol_P5  347 FYVRKI--RFE------GN----------DTSKDAVLRREM---RQMEG---------AWLGSDLV 382

Ana1_P1  261 QEDINAIFGT----GFF----SNVQASP---EDTPLGVRVSFIVQPN 296
Ana1_P2  339 QEGIKELTKRYQDQGYV---LANVVGAPQ----VSENGVVTLQVAEG 378
Ana1_P3  429 QKDLQRVFGT----GLF-ED-VNVSLDP---GTDPTKVNVVVNVVER 466
Ecol_P1   60 SNTIRALFAT----GNF-ED-VRVLRD---------GDTLLVQVKER  91
Ecol_P2  131 ADIEKGLEDFYYSVGKYSAS-VKAVVTP----LPRNRVDLKLVFQEG 172
Ecol_P3  220 AGDLETLRSYYLDRGYARFN-IDSTQVS--LTPDKKGIYVTVNITEG 263
Ecol_P4  302 TKMEDDIKKLLGRYGYAYPR-VQSMPE---INDADKTVKLRVNVDAG 344
Ecol_P5  383 DQGKERLNRL----GFF-ET-VDTDTQ--RVPGSPDQVDVVYKVKER 421
```

Supporting Figure 7 Multiple sequence alignment of POTRA domains of *ana*Omp85 and *ec*BamA. Sequence of individual POTRA domains *ana*Omp85 and *ec*BamA were cut out and a multiple sequence alignment (MSA) was constructed with MAFFT. The MSA was visualized with Jalview using the ClustalX color code (www.jalview.org) (1). Residues, which were mutated to cysteine and spin labelled in this study, are highlighted by a red box.

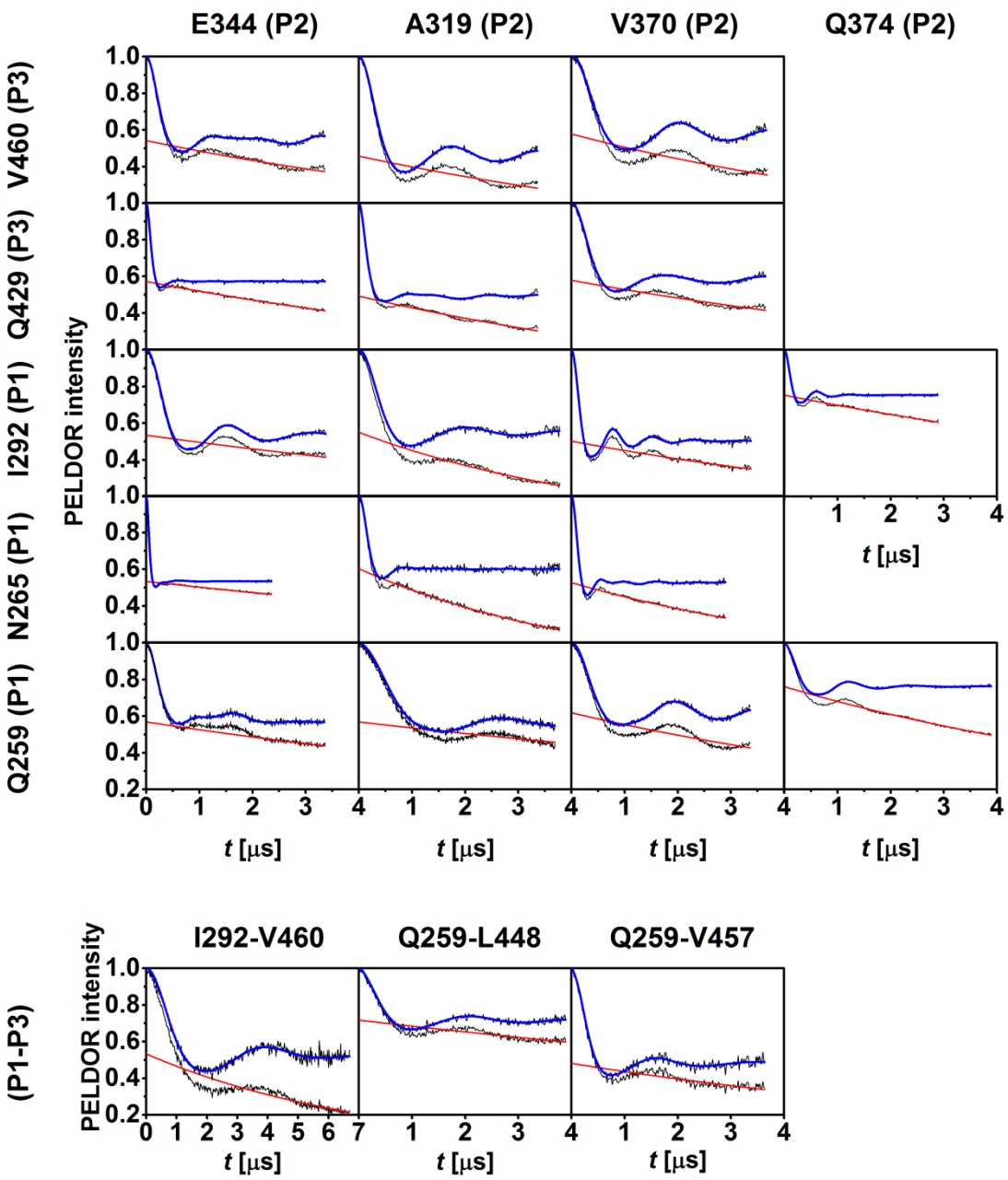

Supporting Figure 8. PELDOR data analysis of inter-POTRA domain distances. The primary and background-corrected PELDOR time traces for measurements on the inter-domain double mutants with fits from Tikhonov regularization (blue) are shown. The 3D-backgrounds are shown in red.

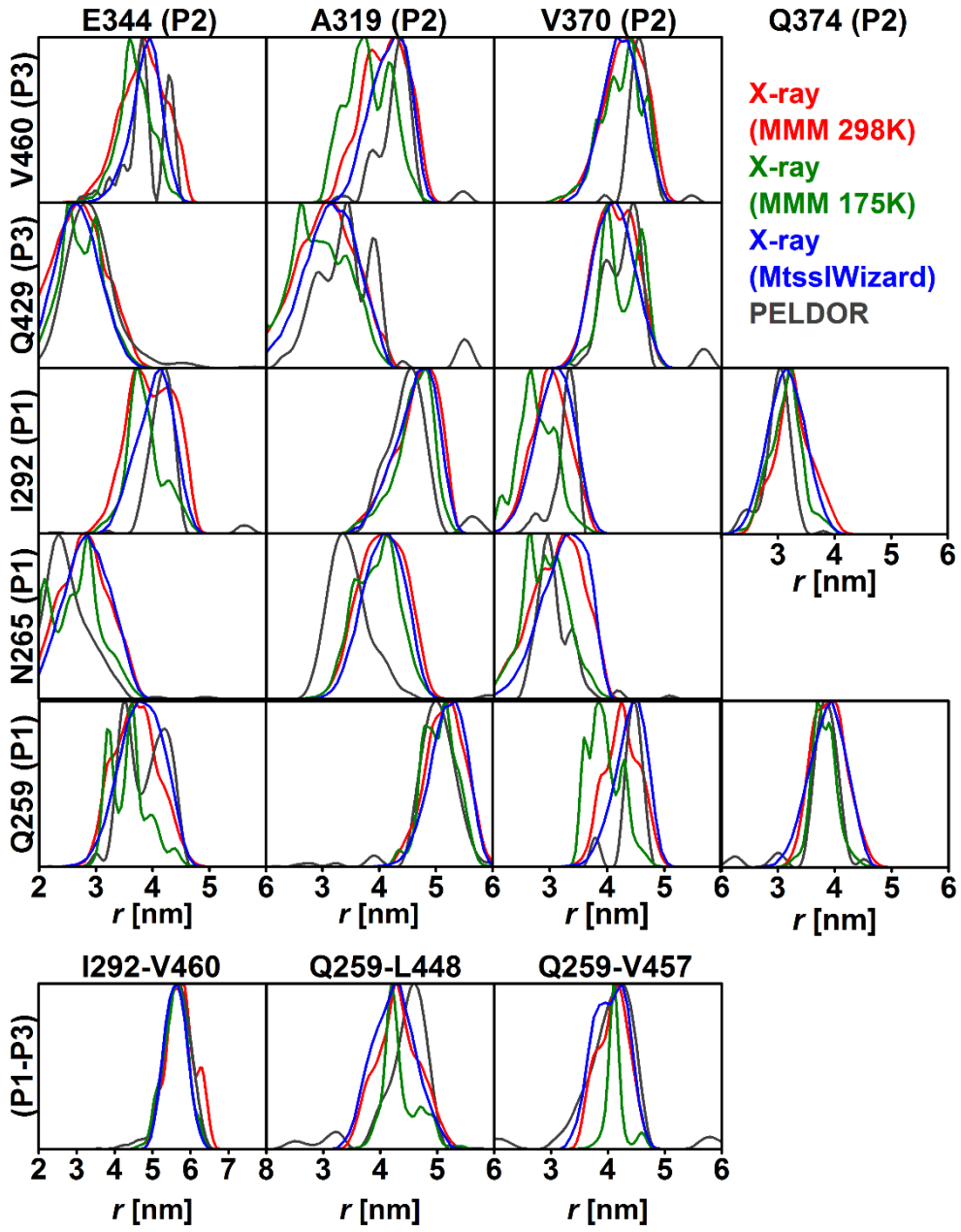

Supporting Figure 9. Comparison of experimentally obtained inter-POTRA domain distance distributions with distributions generated by MMM and MtsslWizard. Distance distributions generated on X-ray structure by MMM in 298 K mode (red), MMM in 175 K mode (green) and mtsslWizard using thorough search and loose vdW restraints (blue) are compared to the obtained distance distributions by Tikhonov regularization (black).

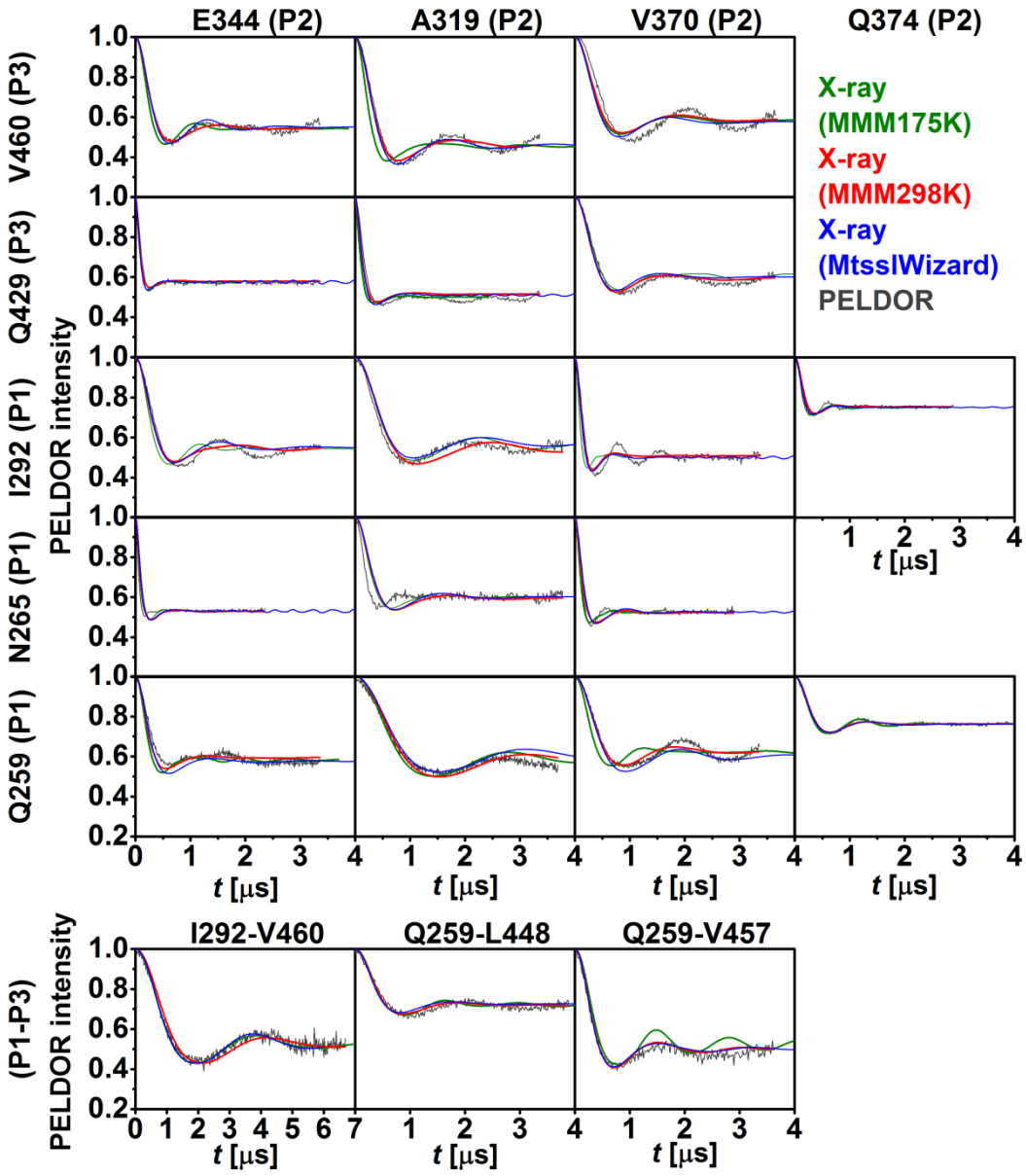

Supporting Figure 10. Comparison of inter-POTRA domain PELDOR time traces generated by MMM and MtsslWizard with experimental traces. Time traces generated on X-ray structure by MMM in 298 K mode (red), MMM in 175 K mode (green) were directly obtained from MMM software package. While time traces for distance distributions from mtsslWizard using thorough search and loose vdW restraints (cutoff 2.5Å, 5 clashes allowed) (blue) were obtained by ha home-written MATLAB® script.

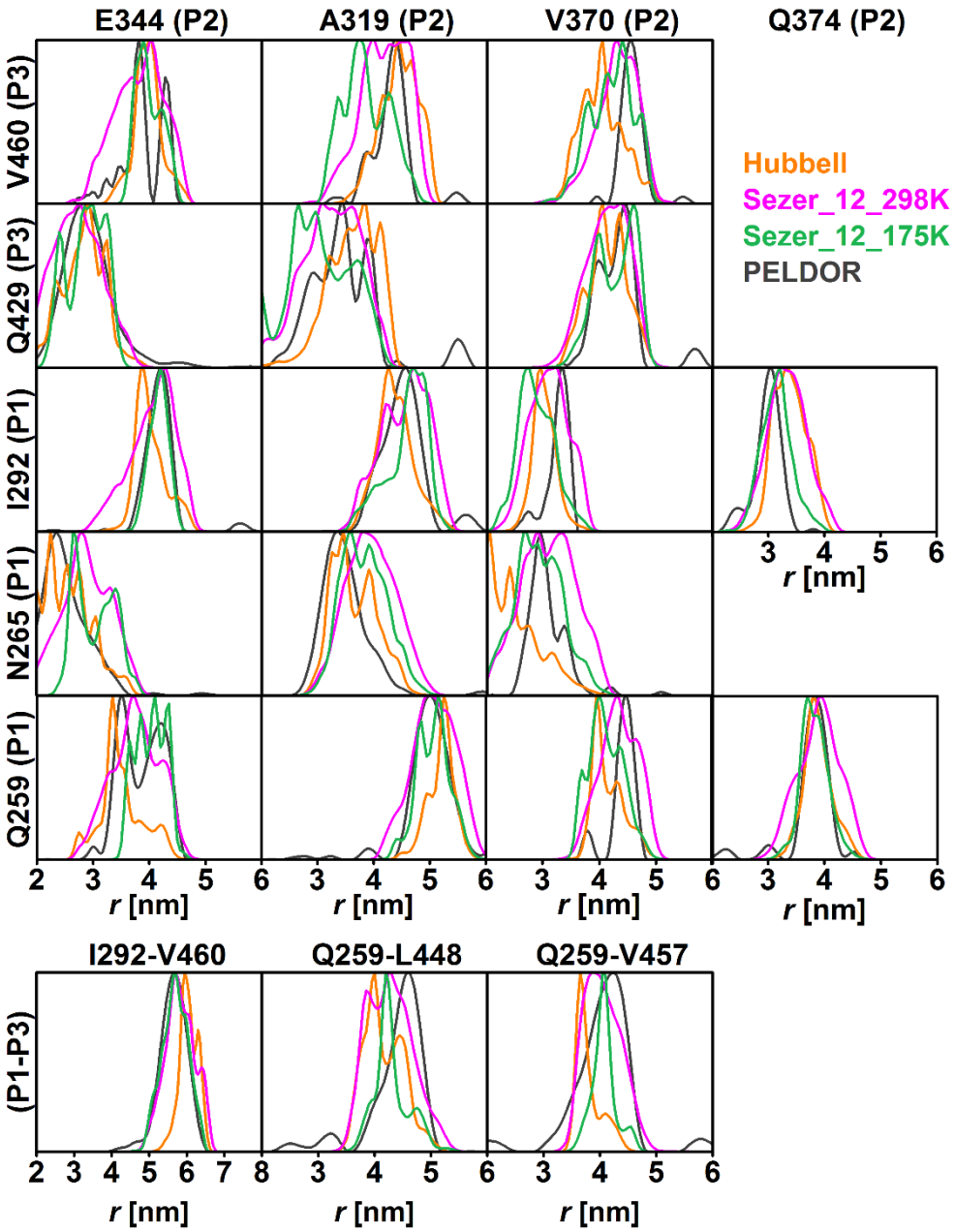

Supporting Figure 11. Comparison of experimentally obtained inter-POTRA domain distance distributions with distance distributions generated by rotamer libraries from Sezer and Hubbell. Distance distributions generated on X-ray structure by MMM using rotamer libraries optimized for chi1 and chi2 angles from Sezer et al. 298 K (magenta) and 175 K (light green) as well as rotamer library from Hubbell et al. (orange).

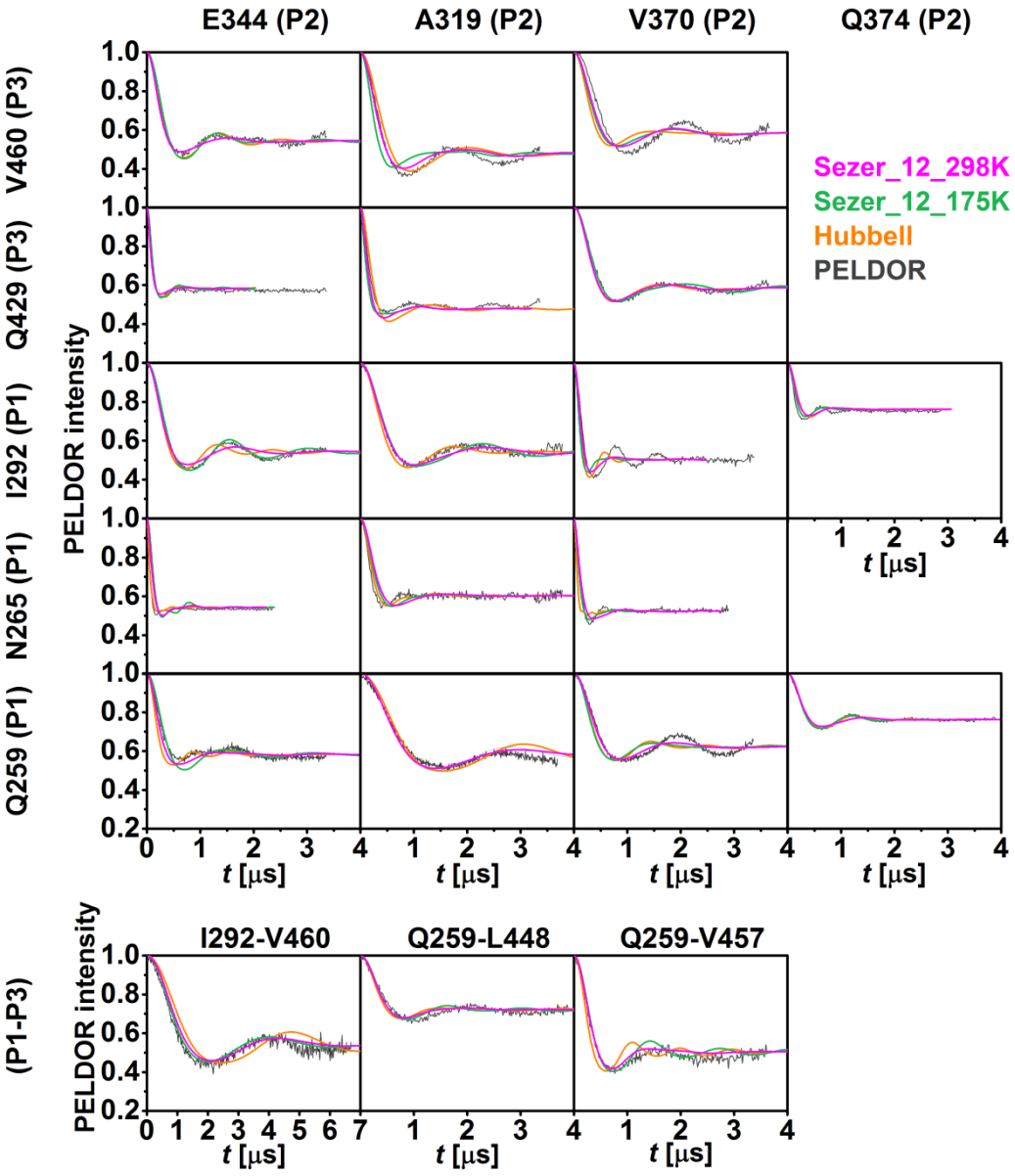

Supporting Figure 12. Comparison of inter-POTRA domain PELDOR time traces generated by rotamer libraries from Sezer and Hubbell. Distance distributions are generated on X-ray structure by MMM using rotamer libraries optimized for chi1 and chi2 angles from Sezer et al. at 298 K (magenta) and 175 K (light green) as well as rotamer library from Hubbell et al. (orange).

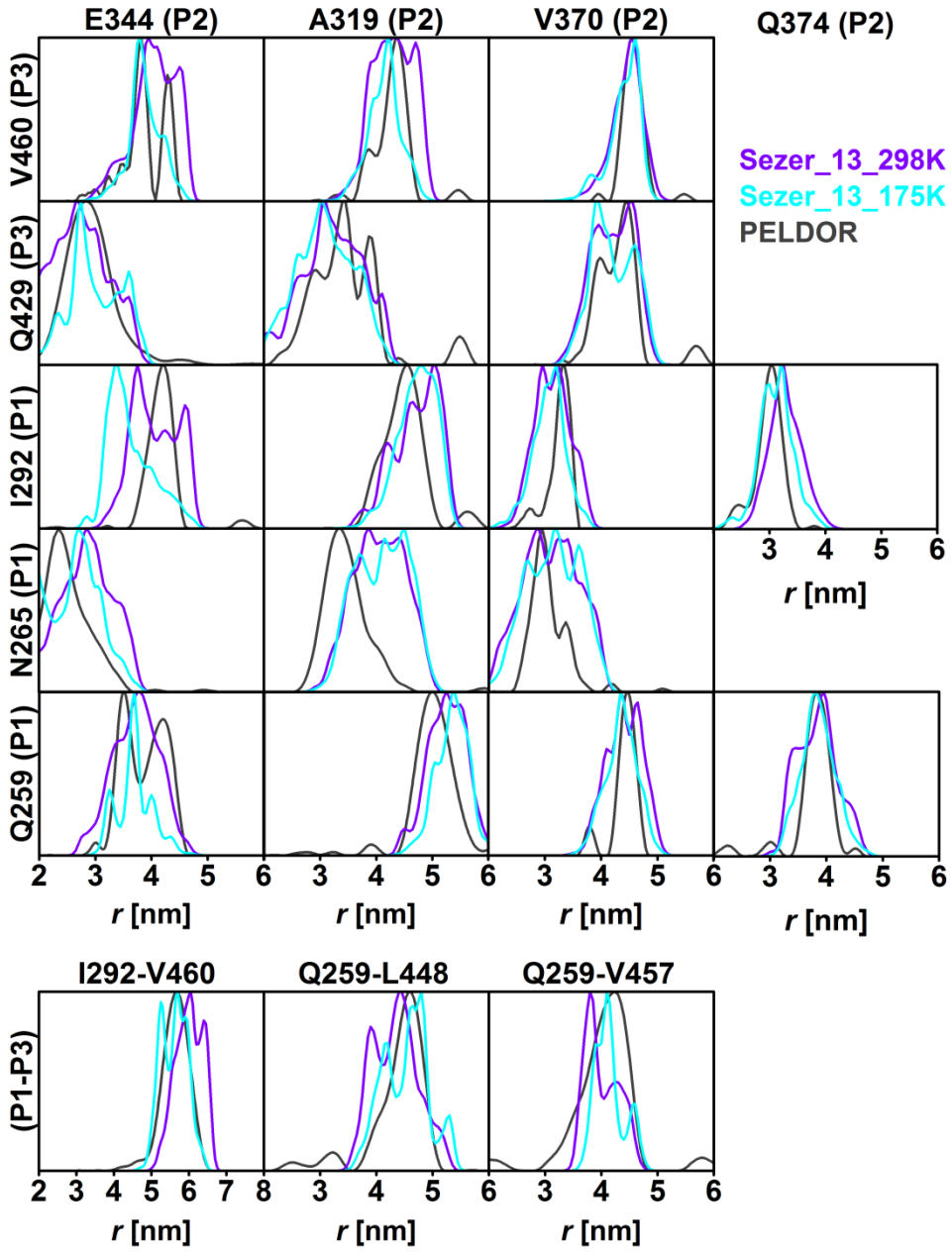

Supporting Figure 13. Comparison of experimentally obtained inter-POTRA domain distance distributions with those generated by rotamer libraries optimized for chi1 and chi3 angles from Sezer. Distributions are generated on X-ray structure using MMM at 298K (violet) and 175K (cyan).

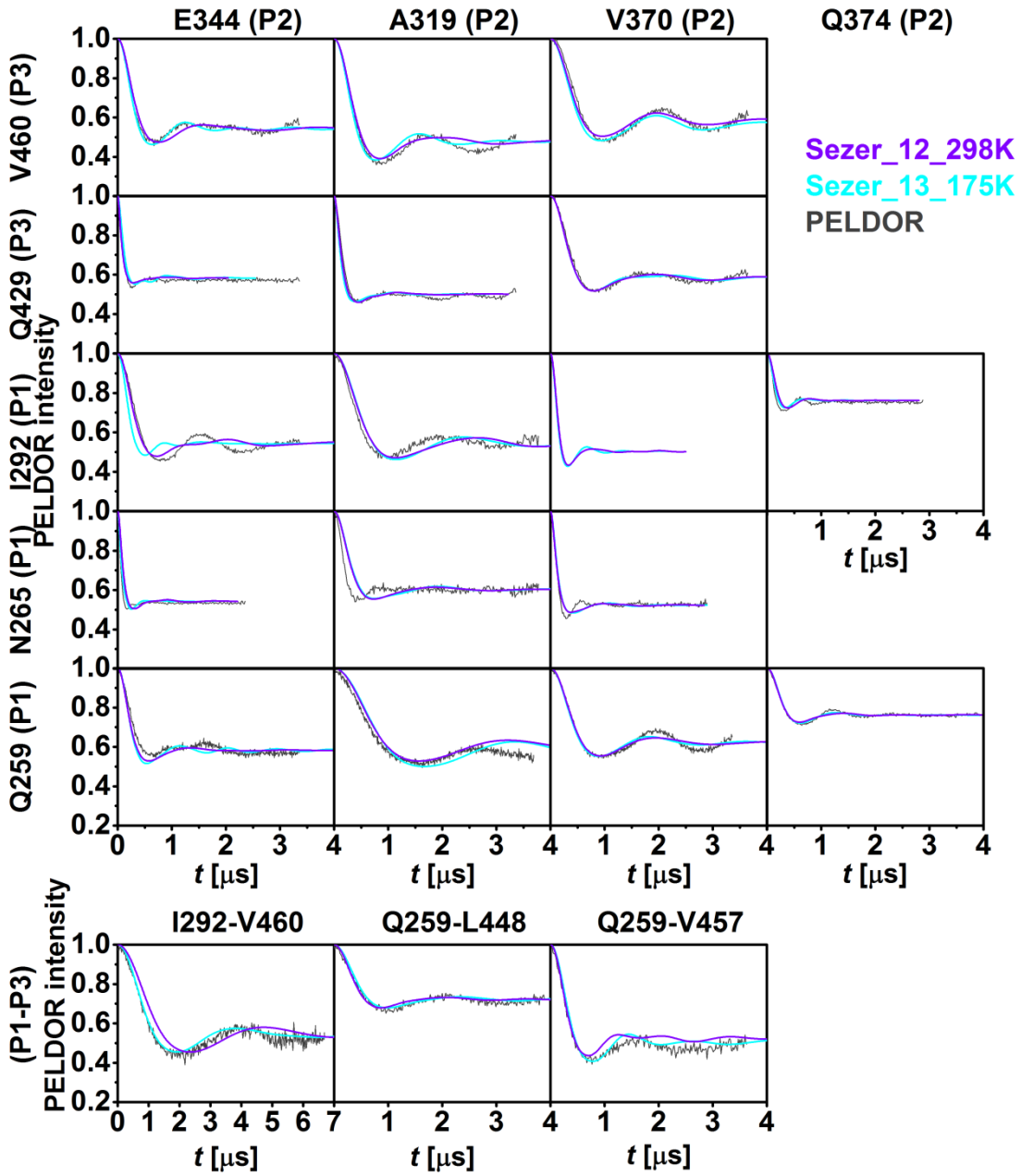

Supporting Figure 14. Comparison of inter-POTRA domain PELDOR time traces generated by rotamer libraries optimized for chi1 and chi3 angles from Sezer. Distance distributions are generated on X-ray structure by MMM using rotamer libraries optimized for chi1 and chi3 from Sezer et al. at 298K (violet) and 175K (cyan).

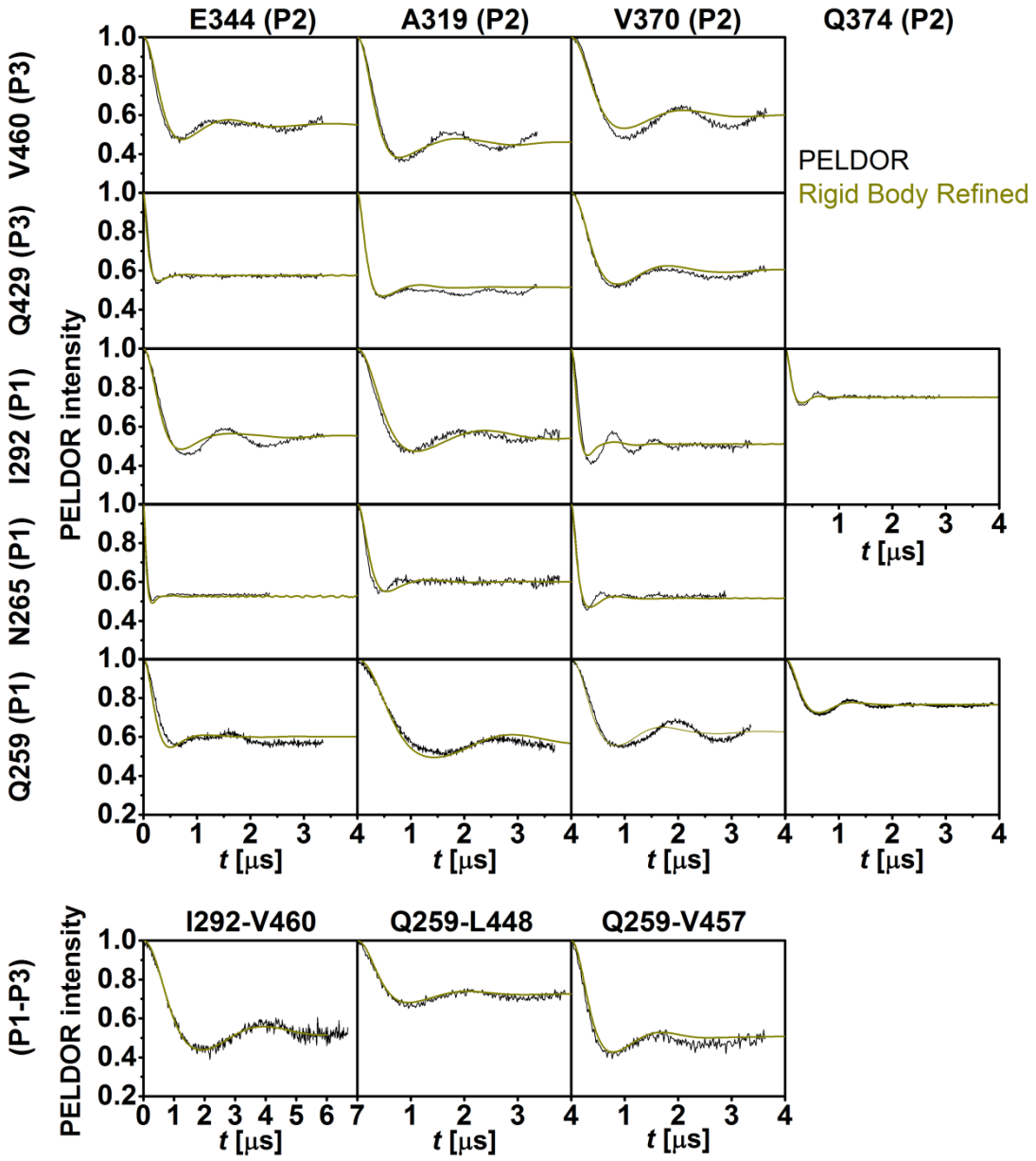

Supporting Figure 15. Comparison of simulated PELDOR time traces from rigid body refinement with experimental traces. Intramolecular dipolar evolution functions for rigid body refinement (dark yellow) are compared to the background-corrected experimental data (black).

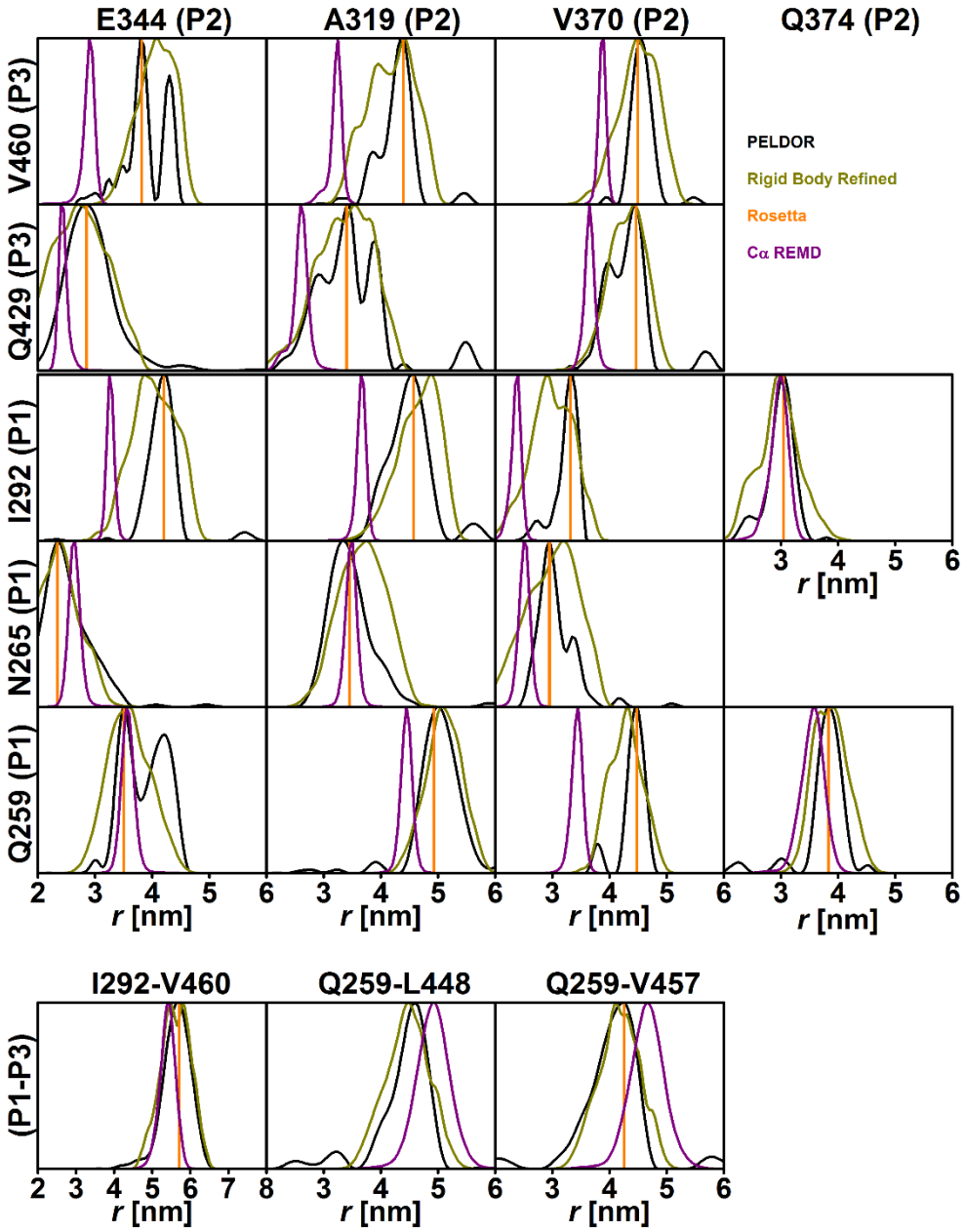

Supporting Figure 16. Comparison of simulated distance distributions from MD simulations and rigid body refinement. Distance distributions for Cα atoms from REMD simulation (violet), are rigid body refinement (dark yellow) are compared to experimentally-obtained data (black). In addition the distances obtained by Rosetta refinement are shown as orange lines. SL pair 259-448 was not included in the Rosetta refinement to avoid a potential clash with neighboring SLs 448, 457 and 460.

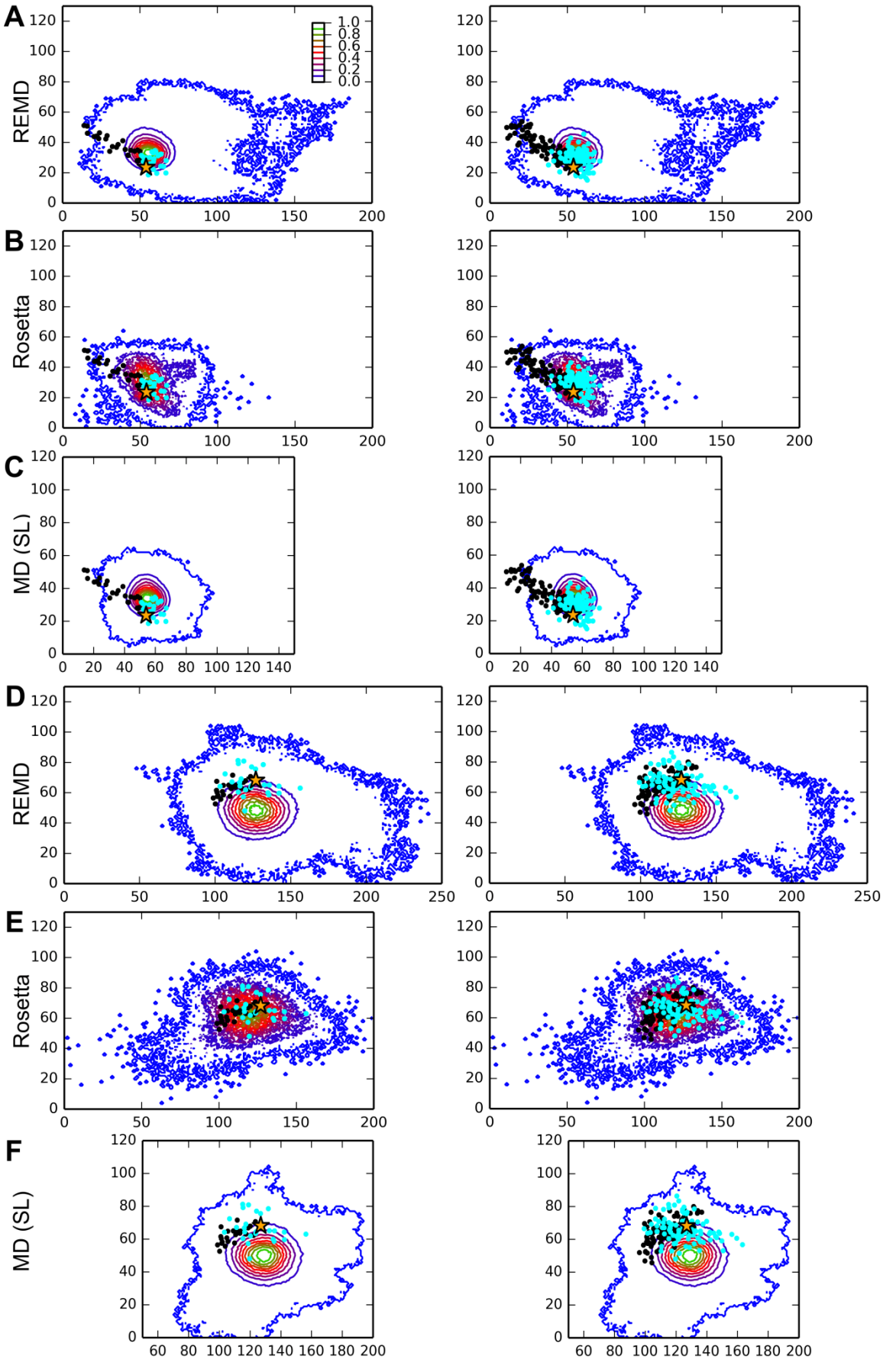
A
REMD
1.0
0.8
0.6
0.4
0.2
0.0
B
Rosetta
C
MD (SL)
D
REMD
E
Rosetta
F
MD (SL)

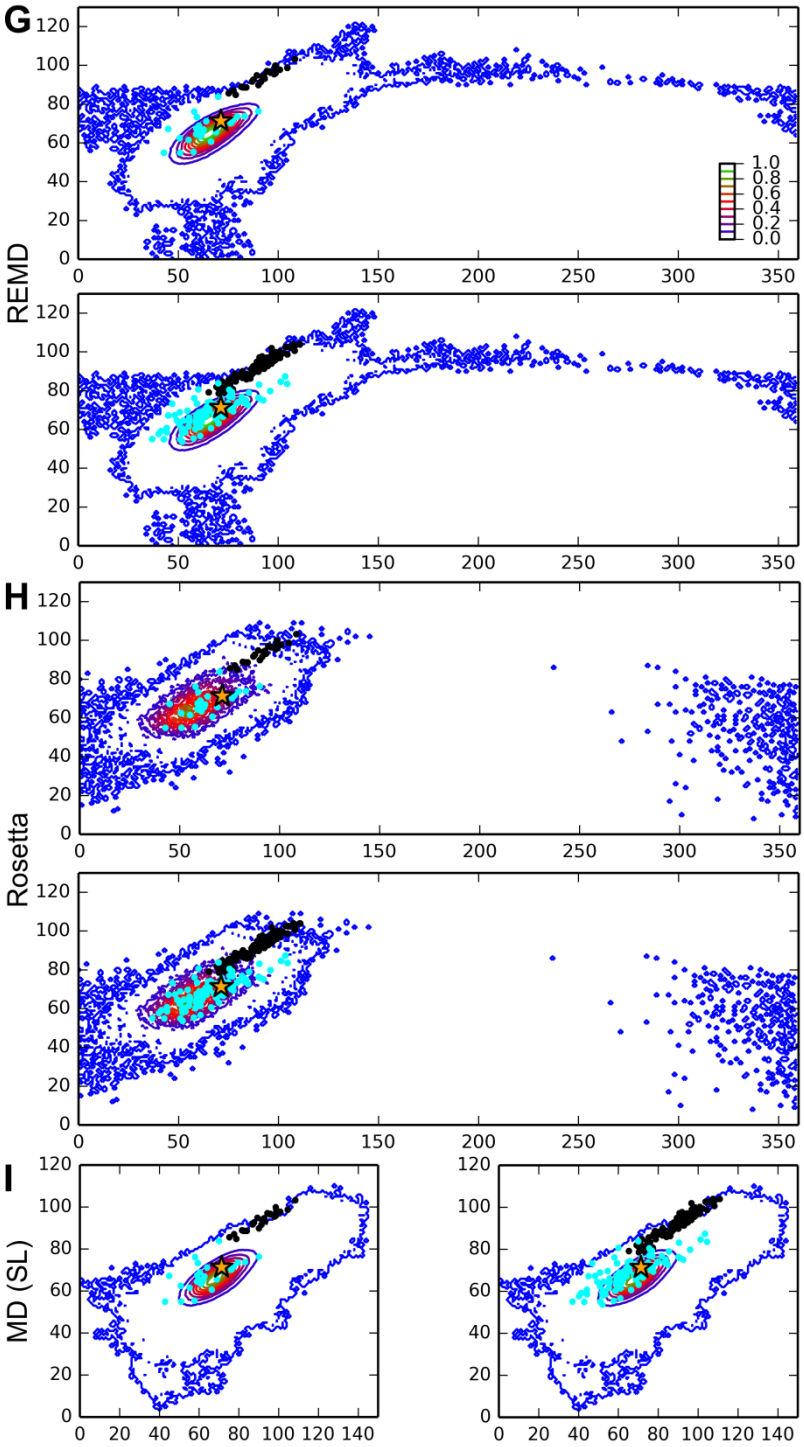

Supporting Figure 17 A-I. Orientational space of POTRA domains of *in silico* spin-labeled Alr2269 sampled by MD simulations and Rosetta. 2D contour plots show the frequency distribution of angular orientations of adjacent POTRA domain pairs of Alr2269 from MD simulations and Rosetta refinement. Just as in Fig. 5 the twist angle is plotted along the x axis and the swing angle along the y axis. (A-C) P2-P3. (D-F) P1-P3. (G-I) P1-P2. The top models from rigid body (filled black circles) and Rosetta (filled cyan circles) refinement are mapped onto the contour plots. In panels A-F, and I the top 25 and top 100 models are shown on the left and right panel, respectively. In panels G and H the upper panel holds the top 25 and the lower panel the top 100 models. In all plots the asterisk indicates the conformation of the respective domains in the X-ray structure.

Supporting Figure 18. Predicted flexibility in POTRA domain pair *ana*P1-*ana*P2. An ensemble of MD structures on the outer contour line of the elliptic region in Fig. 5D, representing the most populated orientations of *ana*P1-*ana*P2 is shown superimposed onto *ana*P2 from two different viewpoints.

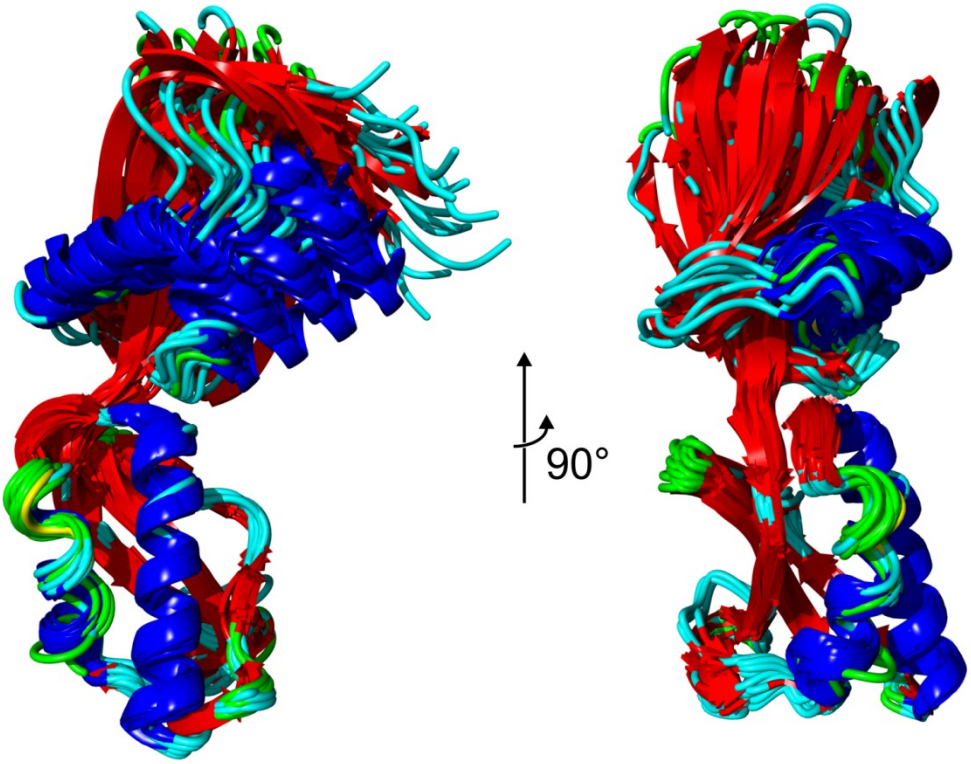

Supporting Table 1. Oligonucleotides used for QuickChange PCR.

NAME	SEQUENCE
V460C	TACAGACCCCACCAAGGTGAATGTGTGCGTAAATGTGGTAGAACGCAGCGTCGAC CACCACCACCACCACCACTGAGATCC
V457C	GGTACGGATCCCACCAAGTGTAATGTGGTGGTAAATGTGGTAG
L448C	GAAGACGTCAATGTTTCCTGTGACCCCGGTACAGACCCCACC
Q429C	GGTATTCAACCGCAACACCGTCTGCAAAGATCTACAACGCGTATTCGGGACAGG
V370C	AGGTTTCCGAAAATGGATGCGTCACCCTGCAAGTAGC
E344C	CAAGAAGGGATTAAGTGCTTAACCAAACGTTATCAAGACC
D337C,D351C	TTCTCAACTTGCGGTGTTTACAAGAAGGGATTAAGGAATTAACCAAACGTTATCAAtg CCAAGGTTACGTTCTCGCC
A319C	GGACTAACGTTCCCTCAGTACTACCCCAGTGTACTGCTGATGAAATTTTCCGCGC
I292C	CGAGTCAGCTTCTGTGTCCAGCCCAACCCCGTC
Q259C	GGACAACCACCCGTTCCTGTTTACAAGAAGATATCAACGCTATC
Q374C	CGCCAATGTTGTAGGaGCtCCCCAGGTTTCCGAAAATGGAGTTGTCACCCTGtgtGTA GCCGAAGGGGTCG
N256C	TTCCCAGTTACAAGAAGATATctgCGCTATCTTTGGCACAGGC

Supporting Table 2. Comparison of PELDOR distance constraints with X-ray structure, MD and the best refined model of either rigid body or Rosetta refinement.

Pair	$\langle r \rangle_{PELDOR}/r_{pk}$ [a]	$\langle r \rangle_{X\text{-}ray}$ [b]	$\langle r \rangle_{MD}$ [c]	$\langle r \rangle_{Rigid\ Body}$ [d]	$\langle r \rangle_{Rosetta}$ [e]
N265-I292	2.3/2.4 (0.3)	2.4 (0.4)	n.d.	n.d.	2.4
A319-D337	2.5/2.6 (0.4)	2.6 (0.4)	n.d.	n.d.	n.d.
A319-E344	2.1/2.0 (0.5)	2.0 (0.4)	n.d.	n.d.	2.0.
A319-V370	2.1/1.8, 2.3 (0.3)	2.1 (0.5)	n.d.	n.d.	1.8.
D337-D351	2.7/2.8 (0.4)	2.4 (0.5)	n.d.	n.d.	n.d.
E344-V370	2.5/2.4 (0.3)	2.7 (0.4)	n.d.	n.d.	2.9
Q429-V460	2.4/2.5 (0.2)	2.2 (0.4)	2.1 (0.4)	n.d.	2.5
I292-A319	4.5/4.6 (0.5)	4.7 (0.4)	4.7 (0.4)	4.7 (0.4)	4.6
I292-E344	4.2/4.2 (0.3)	4.0 (0.4)	4.0 (0.3)	4.0 (0.5)	4.2
I292-V370	3.3/3.4 (0.2)	3.1 (0.3)	3.2 (0.3)	3.0 (0.4)	3.3
N265-A319	3.5/3.4 (0.4)	4.1 (0.4)	4.2 (0.5)	3.7 (0.6)	3.4
N265-E344	2.3/2.4 (0.4)	2.8 (0.4)	2.9 (0.3)	2.3 (0.5)	2.3
N265-V370	3.0/3.0 (0.4)	3.1 (0.5)	3.3 (0.6)	3.0 (0.6)	2.9
Q259-A319	5.3/ 5.0 (0.8)	5.2 (0.4)	5.6 (0.3)	5.1 (0.4)	4.9
Q259-E344	4.3/3.5, 4.2 (1.3)	3.7 (0.4)	3.8 (0.4)	3.6 (0.5)	3.5
Q259-V370	4.5/4.5 (0.5)	4.3 (0.3)	4.7 (0.2)	4.3 (0.4)	4.5
Q374-Q259	3.8/3.8 (0.4)	3.9 (0.3)	n.d.	3.9 (0.4)	3.9
Q374-I292	3.0/3.0 (0.3)	3.3 (0.4)	n.d.	3.0 (0.3)	3.1
V460-A319	4.4/4.4 (0.3)	4.2 (0.4)	4.2 (0.3)	4.2 (0.5)	4.4
V460-E344	3.9/3.8, 4.3 (0.5)	3.9 (0.4)	4.1 (0.4)	4.1 (0.5)	3.8
V460-V370	4.6/4.6 (0.2)	4.3 (0.4)	4.8 (0.3)	4.5 (0.4)	4.5
Q429-A319	3.4/3.4 (0.6)	3.1 (0.5)	3.1 (0.5)	3.4 (0.6)	3.4
Q429-E344	2.9/2.8 (0.5)	2.7 (0.5)	2.9 (0.4)	2.7 (0.7)	2.9
Q429-V370	4.3/4.5 (0.4)	4.1 (0.4)	4.3 (0.3)	4.3 (0.4)	4.5
V460-I292	5.7/5.7 (0.6)	5.7 (0.4)	6.4 (0.3)	5.6 (0.5)	5.7
V457-Q259	4.1/4.2 (0.8)	4.1 (0.3)	4.6 (0.4)	4.2 (0.4)	4.2
L448-Q259	4.3/4.6 (0.7)	4.3 (0.4)	4.7 (0.5)	4.5 (0.4)	4.6

[a] Distances in nm; $\langle r \rangle$ is the mean distance; r_{pk} is the main distance; the standard deviations are given in parentheses.

[b] Distances are predicted by MMM in 298 K mode; the standard deviations are given in parentheses.

[c] Distances are predicted from MD simulations of spin-labeled mutants.

[d] Refined distances obtained from home-written script

[e] Refined distances obtained from Rosetta

Supporting Table 3. Comparison of simulated distance constraints obtained for different rotamer libraries.

Pair	<*r*>X-ray MMM175K	<*r*>X-ray Mtssl-wizard	<*r*>X-ray Sezer12 175K	<*r*>X-ray Sezer12 298K	<*r*>X-ray Sezer13 175K	<*r*>X-ray Sezer13 298K	<*r*>X-ray Hubbell 298K
N265-I292	2.3 (0.4)	2.4 (0.4)	2.3 (0.4)	2.3 (0.4)	2.2 (0.4)	2.3 (0.4)	2.3 (0.3)
A319-D337	2.6 (0.4)	2.5 (0.4)	2.4 (0.4)	2.3 (0.5)	2.6 (0.4)	2.6 (0.4)	2.6 (0.3)
A319-E344	2.0 (0.4)	2.0 (0.4)	1.6 (0.4)	1.9 (0.4)	2.0 (0.3)	2.1 (0.4)	2.4 (0.3)
A319-V370	2.2 (0.4)	2.0 (0.5)	2.1 (0.5)	2.0 (0.5)	2.1 (0.4)	2.1 (0.5)	1.9 (0.4)
D337-D351	2.3 (0.4)	2.3 (0.4)	2.2 (0.4)	2.3 (0.5)	2.2 (0.6)	2.4 (0.5)	2.2 (0.3)
E344-V370	2.6 (0.3)	2.7 (0.3)	2.6 (0.4)	2.6 (0.4)	2.2 (0.5)	2.7 (0.4)	2.8 (0.2)
Q429-V460	2.2 (0.4)	2.2 (0.4)	2.2 (0.4)	2.1 (0.5)	2.1 (0.5)	2.3 (0.4)	2.3 (0.4)
I292-A319	4.6 (0.4)	4.6 (0.4)	4.6 (0.4)	4.5 (0.4)	4.7 (0.4)	4.7 (0.4)	4.4 (0.3)
I292-E344	3.9 (0.3)	4.0 (0.3)	4.2 (0.7)	4.0 (0.4)	3.6 (0.4)	4.0 (0.4)	4.0 (0.3)
I292-V370	2.8 (0.3)	3.1 (0.3)	2.9 (0.3)	3.3 (0.4)	3.1 (0.3)	3.1 (0.3)	3.0 (0.2)
N265-A319	3.9 (0.4)	4.1 (0.4)	3.8 (0.4)	3.9 (0.4)	4.1 (0.5)	4.0 (0.4)	3.6 (0.4)
N265-E344	2.7 (0.4)	2.8 (0.4)	3.0 (0.4)	2.9 (0.5)	2.6 (0.5)	2.8 (0.5)	2.4 (0.5)
N265-V370	2.9 (0.4)	3.2 (0.4)	2.9 (0.4)	3.1 (0.5)	3.1 (0.5)	3.1 (0.5)	2.5 (0.5)
Q259-A319	5.1 (0.3)	5.2 (0.3)	5.1 (0.3)	5.1 (0.4)	5.3 (0.3)	5.2 (0.4)	2.5 (0.6)
Q259-E344	3.6 (0.4)	3.8 (0.4)	4.0 (0.3)	3.7 (0.4)	3.7 (0.3)	3.7 (0.4)	3.5 (0.4)
Q259-V370	4.0 (0.3)	4.4 (0.3)	4.1 (0.3)	4.3 (0.3)	4.3 (0.3)	4.4 (0.3)	4.2 (0.3)
Q374-Q259	3.8 (0.2)	3.9 (0.3)	3.8 (0.3)	3.9 (0.4)	3.8 (0.4)	3.8 (0.4)	3.9 (0.3)
Q374-I292	3.1 (0.3)	3.2 (0.4)	3.2 (0.3)	3.3 (0.4)	3.3 (0.3)	3.3 (0.3)	3.4 (0.3)
V460-A319	3.9 (0.4)	4.2 (0.3)	3.8 (0.4)	4.2 (0.4)	4.1 (0.3)	4.3 (0.4)	4.4 (0.4)
V460-E344	3.8 (0.3)	3.9 (0.3)	4.0 (0.2)	3.8 (0.4)	3.9 (0.3)	4.0 (0.4)	4.0 (0.3)
V460-V370	4.2 (0.4)	4.2 (0.3)	4.2 (0.4)	4.3 (0.4)	4.4 (0.3)	4.4 (0.3)	4.0 (0.4)
Q429-A319	2.9 (0.6)	3.1 (0.5)	3.0 (0.6)	3.2 (0.5)	3.1 (0.5)	3.2 (0.5)	3.6 (0.4)
Q429-E344	2.7 (0.4)	2.7 (0.4)	2.9 (0.3)	2.7 (0.5)	3.0 (0.5)	2.7 (0.6)	2.8 (0.4)
Q429-V370	4.2 (0.4)	4.1 (0.4)	4.3 (0.4)	4.1 (0.4)	4.2 (0.4)	4.2 (0.4)	4.1 (0.4)
V460-I292	5.6 (0.3)	5.6 (0.3)	5.7 (0.4)	5.8 (0.4)	5.6 (0.4)	6.0 (0.4)	6.0 (0.3)
V457-Q259	4.1 (0.2)	4.0 (0.3)	4.2 (0.2)	4.0 (0.3)	4.1 (0.3)	4.0 (0.3)	3.8 (0.3)
L448-Q259	4.4 (0.3)	4.2 (0.4)	4.3 (0.3)	4.3 (0.4)	4.5 (0.4)	4.3 (0.4)	4.2 (0.4)

Supporting Table S4. Structural similarities of POTRA domains of *ana*Omp85 and *ec*BamA. For each POTRA pair (PDB: 3mc8, 5ayw) the Cα RMSD [Å] after structural alignment with YASARA's MUSTANG plugin was determined. The background color gives the degree of similarity from white lowest similarity and black highest similarity.

	anaP2	anaP3	ecP1	ecP2	ecP3	ecP4	ecP5
anaP1	1.966	1.006	1.056	1.561	1.437	1.367	1.279
anaP2		1.707	2.009	2.023	1.597	1.665	1.888
anaP3			1.186	1.941	1.748	1.670	1.209
ecP1				1.443	1.490	1.463	1.300
ecP2					1.515	1.768	1.582
ecP3						1.580	1.503
ecP4							1.387

Supporting Table S5. Angles and scores of top 100 Rosetta models.

Twist and swing angles are given in columns 1-4 for adjacent POTRA domain pairs, in columns 5 and 6 for P1-P3. The last two columns hold the Rosetta score and the distance constraint score. [a] The score in column 7 was calculated by subtracting the atom pair constraint score from the total score. [b] The distance constraint score in column 8 was calculated as follows: $\frac{atom\ pair\ constraint\ score}{constraint\ score\ weight * number\ of\ constraints}$ with a weight of 4 and in total 24 constraints.

Twist (P1-P2)	Swing (P1-P2)	Twist (P2-P3)	Swing (P2-P3)	Twist (P1-P3)	Swing P1-P3)	Rosetta score[a]	distance constraint score[b]
66.4	60.6	52.2	27.3	119.6	48.0	-427.232	0.9762
62.7	66.9	50.9	31.5	117.2	69.1	-428.915	0.9746
59.3	73.3	65.4	24.1	126.8	75.6	-433.18	0.9745
76.2	70.1	58.8	22.2	135.6	58.6	-426.902	0.9742
62.2	65.6	53.8	29.9	118.7	57.3	-424.715	0.9742
60.9	63.4	56.5	25.9	120.2	61.9	-431.877	0.974
45.0	67.2	60.9	19.6	106.6	72.4	-425.407	0.974
90.0	76.3	61.7	31.2	156.3	63.0	-434.098	0.974
50.7	62.4	63.5	24.3	116.2	66.7	-426.334	0.9739
68.8	65.6	59.7	34.6	132.5	65.2	-430.368	0.9739
60.7	65.3	58.5	33.1	123.6	63.4	-430.716	0.9737
79.5	73.6	53.3	25.9	135.9	65.0	-438.231	0.9736
71.3	69.7	60.3	33.9	135.0	59.9	-428.997	0.9734
42.8	54.9	56.3	30.0	103.3	64.2	-429.479	0.9734
77.3	71.5	62.9	31.9	142.2	64.3	-432.622	0.9734
59.0	67.5	53.4	29.1	115.3	60.4	-424.882	0.9731
60.4	68.9	53.2	28.2	116.4	64.4	-427.321	0.973
55.2	61.5	67.0	28.0	119.0	80.9	-434.847	0.9729
58.9	64.5	58.8	27.3	115.4	79.2	-430.594	0.9728
83.1	73.8	57.8	33.8	142.3	59.7	-431.497	0.9728
58.0	76.1	55.5	18.6	115.2	81.2	-427.361	0.9726
70.0	83.8	51.8	30.7	124.1	77.0	-424.906	0.9726
64.0	71.1	66.8	19.8	131.8	78.5	-446.642	0.9726
50.9	54.9	59.0	29.2	111.1	67.1	-438.485	0.9726
57.7	55.4	63.8	32.3	123.8	64.4	-427.586	0.9725
77.4	69.3	62.9	15.1	137.8	58.1	-426.479	0.9725
73.2	71.7	57.6	24.6	130.8	62.7	-435.525	0.9725
60.0	80.7	45.1	20.6	106.7	78.9	-424.411	0.9725
44.2	60.7	60.7	17.8	107.7	64.8	-428.938	0.9724
61.0	56.7	66.2	32.1	129.5	64.1	-425.634	0.9724
65.3	71.7	60.4	26.8	128.2	70.2	-430.184	0.9723
58.9	63.0	49.5	30.8	112.4	67.1	-435.095	0.9722
103.4	87.4	53.1	36.2	159.5	60.6	-438.027	0.9722
54.6	69.6	63.4	27.7	121.8	83.4	-429.475	0.9721
52.0	58.0	62.8	27.9	115.4	70.2	-426.927	0.9721
61.0	63.2	62.5	35.1	124.2	78.2	-433.354	0.972

72.4	66.6	51.3	34.5	126.4	55.6	-434.568	0.972
101.2	84.6	45.7	29.9	147.8	64.4	-435.971	0.9719
52.6	64.6	62.1	16.3	111.8	78.2	-430.736	0.9718
72.4	68.6	41.2	27.8	115.7	65.8	-429.313	0.9718
92.5	75.1	52.9	35.7	149.8	59.1	-432.275	0.9718
75.5	77.0	49.5	27.2	125.0	66.9	-428.126	0.9718
41.4	59.2	63.0	22.1	108.8	70.9	-426.711	0.9718
69.1	65.9	48.5	28.9	119.7	57.6	-430.954	0.9717
49.4	64.5	55.3	26.0	107.6	68.2	-424.655	0.9717
65.9	74.2	57.2	27.6	125.2	79.6	-429.128	0.9717
60.4	63.0	57.6	32.7	121.8	63.8	-434.068	0.9717
84.7	72.7	56.0	32.9	145.7	61.8	-436.232	0.9716
71.6	75.8	53.1	34.3	128.0	60.3	-425.779	0.9716
61.7	66.0	45.1	33.2	110.2	52.8	-425.604	0.9716
76.3	70.4	52.8	32.2	131.8	57.3	-438.73	0.9715
55.5	63.9	64.0	23.5	121.7	60.7	-428.583	0.9714
62.6	69.4	62.5	30.5	128.2	70.1	-425.372	0.9714
79.9	74.1	49.3	33.0	132.9	64.9	-425.776	0.9714
59.1	65.9	50.6	40.3	117.1	52.9	-424.811	0.9713
52.0	53.7	60.8	37.3	118.1	62.4	-426.632	0.9713
50.8	68.9	63.7	19.7	116.1	67.3	-428.57	0.9713
40.2	57.7	64.1	27.5	107.5	64.7	-424.968	0.9712
53.5	58.5	58.3	25.5	111.8	70.1	-434.722	0.9712
90.9	75.8	55.5	28.1	148.3	63.6	-434.23	0.9712
61.2	65.2	61.5	30.0	125.4	68.6	-427.366	0.9712
66.3	73.2	56.0	30.5	125.8	68.0	-436.535	0.9711
58.5	60.2	67.5	33.5	131.2	62.5	-424.536	0.9711
75.5	80.5	56.0	25.0	130.3	65.9	-431.546	0.9711
64.3	69.6	60.7	28.7	127.7	65.9	-428.73	0.9711
48.3	67.3	63.0	21.1	112.5	72.3	-426.236	0.971
81.8	76.8	54.1	30.8	141.7	63.3	-438.085	0.971
64.6	71.0	57.5	35.8	125.2	76.0	-425.252	0.9709
74.8	73.6	57.2	26.8	134.0	70.6	-436.696	0.9709
64.9	73.0	59.0	30.1	126.8	68.1	-430.512	0.9709
85.3	78.9	52.4	36.6	135.2	53.2	-429.014	0.9709
63.9	67.9	59.0	31.4	126.1	67.8	-426.678	0.9708
67.8	67.6	55.6	18.0	123.8	62.4	-425.551	0.9707
77.0	76.6	58.4	30.2	139.9	70.9	-427.618	0.9707
51.8	59.4	60.6	45.5	122.1	51.5	-424.932	0.9707
61.0	61.4	37.8	25.1	101.5	63.7	-429.836	0.9707
76.8	79.3	55.3	28.5	137.6	69.3	-425.145	0.9706
55.5	66.1	59.8	34.5	120.0	68.6	-424.392	0.9705
72.4	67.1	59.0	33.6	136.2	63.4	-434.194	0.9705
70.1	63.1	59.7	33.8	134.1	60.8	-424.863	0.9705
65.6	69.7	58.7	17.4	126.0	71.4	-435.61	0.9704
61.7	64.2	56.9	30.4	121.8	65.5	-425.225	0.9704
104.5	83.5	56.6	34.5	163.2	56.7	-434.33	0.9704
64.1	67.2	59.1	27.0	125.8	64.1	-433.017	0.9704
68.4	72.9	39.8	34.0	110.6	55.7	-427.262	0.9704
73.5	72.6	48.6	27.6	124.0	71.0	-432.072	0.9704
83.7	75.1	55.4	32.4	144.5	63.8	-431.852	0.9704
69.4	66.5	55.2	30.3	128.3	61.9	-428.559	0.9704
37.0	55.1	57.2	33.3	99.2	66.5	-424.334	0.9704
90.4	83.1	50.6	37.5	146.4	61.0	-433.895	0.9703
46.9	73.3	71.0	27.7	120.5	86.4	-424.909	0.9703
67.7	72.8	57.2	40.3	130.7	64.0	-426.182	0.9703
75.6	72.0	46.3	29.5	124.4	67.5	-430.156	0.9703
52.3	60.3	55.9	31.8	112.4	63.3	-428.166	0.9703
44.2	58.6	56.0	28.0	103.9	69.2	-428.226	0.9702
55.5	65.2	64.5	19.9	121.4	60.1	-426.885	0.9702
69.9	67.2	58.9	29.7	130.4	71.1	-428.71	0.9702
59.2	64.0	63.6	39.1	128.7	55.1	-424.386	0.9701
64.7	73.9	60.6	25.9	127.1	76.5	-430.707	0.9701
96.0	79.8	52.2	42.9	150.7	53.1	-424.451	0.9701

Supporting References

1. Waterhouse, A. M., J. B. Procter, D. M. A. Martin, M. Clamp, and G. J. Barton. 2009. Jalview Version 2—a multiple sequence alignment editor and analysis workbench. Bioinformatics 25:1189-1191.